Nuclear Physics A529 (1991) 1–19
North-Holland

TRIAXIAL ROTOR PLUS PARTICLE DESCRIPTION OF NEGATIVE-PARITY STATES IN ^{125}Xe

D. LIEBERZ[1], A. GELBERG[1], A. GRANDERATH[1], P. von BRENTANO[1], I. RAGNARSSON[2] and P.B. SEMMES[2,3]

[1] *Institut für Kernphysik der Universität zu Köln, Zülpicherstr. 77, D-5000 Köln, Germany*
[2] *Department of Mathematical Physics, Lund, Institute of Technology, S-22100 Lund, Sweden*
[3] *Physics Department, Tennessee Technological University, Cookeville, TN 38505, USA*

Received 19 October 1990
(Revised 3 January 1991)

Abstract: Excitation energies and branching ratios in ^{125}Xe have been correctly described by using the triaxial rotor plus particle model with deformation parameter $\varepsilon = 0.25$ and $\gamma = 24°$. The observed properties, in particular the degeneracy of the yrast favoured and unfavoured bands and the signature inversion in the yrare bands are well described by the model. The distribution of core states in the wave functions has been calculated. This distribution has been used in interpreting the signature inversion and the staggering in B(E2) and B(M1) which have been predicted by the model.

1. Introduction

The description of odd-A transitional nuclei with masses around $A = 130$ has made little progress until recently, owing to both the lack of sufficient experimental information and the inadequacy of simple models. Due to the progress of in-beam gamma-ray spectroscopy, rather rich information is now available. On the theoretical side, the rotor plus particle model has been extended by including the gamma deformation [1–5]). The interacting boson-fermion model has also been applied to odd nuclei in this region [6,7]).

The even-even Xe nuclei have been described by the gamma soft rotor model [8]) and by the O(6) limit of the interacting boson model [9–11]). It has also been shown that the ground and gamma band of a nucleus with O(6) dynamic symmetry exhibits a definite similarity with a rigid rotor with $\gamma = 30°$ [refs. [10,11])]. In a correct description, based on the Bohr hamiltonian [10]), one has to consider the deformation parameter γ as a dynamic variable. The assumption of a rigid core is equivalent to replacing γ by some effective value. The validity of this assumption has been discussed by Leander [12]).

The aim of the present research is to examine whether there are features of the excited states of odd-A Xe which can be explained only if a triaxial description is assumed. Although alternative descriptions are provided by boson models [6,7,13]), this discussion will be restricted to the framework of the rigid rotor plus particle

0375-9474/91/$03.50 © 1991 - Elsevier Science Publishers B.V. (North-Holland)

model [1-5,14]) (in what follows "rigid" is used only to indicate a fixed shape; it has no implication for the moments of inertia). We will examine those properties which specifically point to a deviation from axial symmetry.

2. The model

A complete description of the rigid triaxial rotor plus particle (RTRP) model can be found in refs. [3,4]). The hamiltonian is written

$$H = H_{\text{core}} + H_{\text{sp}} + H_{\text{pair}} . \tag{1}$$

The single-particle Hamiltonian H_{sp} comprises a potential [5])

$$U = \tfrac{1}{2}\hbar\omega_0\rho^2\left\{1 - \tfrac{2}{3}\varepsilon\sqrt{\tfrac{4}{5}\pi}\left[\cos\gamma\, Y_{20} - \frac{\sin\gamma}{\sqrt{2}}(Y_{22} + Y_{2-2})\right]\right\}$$
$$- \kappa\hbar\omega_0^0\{2\boldsymbol{l}_t \cdot \boldsymbol{s} + \mu(l_t^2 - \langle l_t^2\rangle_N)\} , \tag{2}$$

where ε and γ are measures of the quadrupole deformation and the triaxiality, respectively. Note that the radius ρ and the orbital angular momentum $\boldsymbol{l}_t$ are both expressed in stretched coordinates.

The eigenfunction of H_{sp} can be written

$$|\Psi_\nu\rangle = \sum_{Nlj\Omega} C^{(\nu)}_{Nlj\Omega} |Nlj\Omega\rangle \tag{3}$$

with Ω, the projection quantum number on the intrinsic axis-3, restricted to $\ldots \frac{3}{2}, \frac{1}{2}, \frac{5}{2}, \ldots$; Nlj are the usual shell-model quantum numbers. The superscript ν simply labels the different deformed single-particle states. The single-particle basis is defined in the stretched coordinate system, so in principle we should add an index "t" to all quantum numbers, but from here on, we will drop this index. Pairing is introduced via a standard BCS procedure, so that the single-particle energies are replaced with quasiparticle energies and appropriate pairing factors are attached to all single-particle matrix elements. The hamiltonian of the rigid rotor can be written

$$H_{\text{core}} = \sum_i \frac{\hbar^2}{2\Theta_i} R_i^2 = \sum_i \frac{\hbar^2}{2\Theta_i}(I_i - j_i)^2 , \tag{4}$$

where $\boldsymbol{R}$ is the core angular momentum which can be expressed through the total angular momentum $\boldsymbol{I}$ and the particle angular momentum $\boldsymbol{j}$. The moments of inertia are assumed to be of hydrodynamical type

$$\Theta_k = \tfrac{4}{3}\Theta_0 \sin^2(\gamma + \tfrac{2}{3}\pi k) . \tag{5}$$

The strong coupling basis states of the complete system $|IMK\nu\rangle$ are labelled by the projection K of I on the intrinsic axis-3 (quantization axis); due to triaxiality, the relation $K = \Omega$ is no longer valid. The calculations have been extended to include the variable moment of inertia (VMI) of the core [2,15]). This is achieved by transforming from the strong coupling basis to the weak coupling basis $|IMR\alpha Nlj\rangle$. In this

basis, the core angular momentum R and particle angular momentum j are good quantum numbers, while α labels core states having the same R. It is then straightforward to calculate the core matrix elements as

$$\langle IMK\nu|H_{\text{core}}|IMK'\nu'\rangle = \sum_{R\alpha Nj} E_{R\alpha}\langle IMK\nu|IMR\alpha Nlj\rangle\langle IMR\alpha Nlj|IMK'\nu'\rangle . \quad (6)$$

Details on the VMI procedure can be found in appendix A.

The electromagnetic transitions considered are M1 and E2. The M1 operator is written as

$$\mathcal{M}(\text{M1}) = \sqrt{\frac{3}{4\pi}}(g_R\boldsymbol{R} + g_l\boldsymbol{l} + g_s\boldsymbol{s}) , \quad (7)$$

where g_R, g_l and g_s are the core, orbital and spin g-factors, respectively. The E2 operator is written schematically

$$\mathcal{M}(\text{E2}, \mu) = \sum_i q_i r_i^2 Y_{2\mu}(\vartheta_i\varphi_i) , \quad (8)$$

where the sum extends over all nucleons and thus splits naturally into contributions from the odd particle and the remaining nucleons (the core). In the present application, the core contribution is given by the usual intrinsic E2 moments Q_0 and Q_2, which are defined in terms of the shape variables ε and γ. The M1 and E2 matrix elements have been given in ref. [3]).

The Nilsson parameters κ, μ as well as the pairing strength G have been given standard values taken from refs. [16,17]) respectively. Note, however, that the Fermi level and the pairing gap are derived quantities and not adjustable parameters. The VMI parameters have been chosen so that the energy of the core 2^+ state is 300 keV; the moment of inertia increases slowly with spin according to the VMI prescription [2,15]) reaching 90% of its original value at $R = 8$ and 80% at $R = 14$. A good agreement between theory and experiment is obtained at $\varepsilon = 0.25$, $\gamma = 24°$. These shape parameters were not determined by any selfconsistency procedure, but simply by an overall fit to the data. No Coriolis attenuation is introduced. In table 1 the used parameters are listed and a short description of the parameters is given in appendix A.

In the particle plus rotor formalism only the shape of the core matters and consequently γ can be restricted to the (0°–60°) interval. Therefore, only the values of the three moments of inertia are important, but not which one is chosen as Θ_1, Θ_2 and Θ_3, respectively. With the Lund convention, this means that the 1-axis is the shorter axis equal to the 2-axis for $\gamma = 0°$ while the 2- and 3-axes become equal for $\gamma = 60°$. With the irrotational variation of the momenta of inertia, eq. (5), this means that Θ_2 is the larger moment of inertia so that at very high spin, the rotation vector will essentially coincide with the 2-axis.

TABLE 1

Input and fit parameters of RTRP and VMI-RTRP

Deformation parameter	$\varepsilon = 0.25$	
Deformation parameter	$\gamma = 24°$	
Inertial parameter (E(2^+; core))	E2PLUS = 0.30 MeV	
Pairing parameter	$G0 = 19.2$ MeV	standard
Pairing parameter	$G1 = 7.40$ MeV	standard
Coriolis attenuation factor (ξ)	CHSI = 1	i.e. no attenuation
VMI parameter	$A00 = 0.036$ MeV	only VMI-RTRP
VMI parameter	STIFF = 0.1 MeV^3	only VMI-RTRP
Effective spin g factor ($g = g_0 \cdot g_{free}$):	$g_0 = 0.6$	standard: $g_0 \approx 0.6$–0.7
Considered orbitals	no. 11–25	

3. Comparison with the experiment

3.1. ENERGIES

Calculations with the RTRP model have been carried out for $^{123-131}$Xe and $^{127-131}$Ba; the complete set of results will be given in a subsequent publication. We will concentrate our discussion on the negative-parity states of ^{125}Xe which has been the object of recent in-beam gamma-ray spectroscopy experiments [18]). A comparison of the experimental and calculated energy levels of ^{125}Xe is shown in fig. 1. States have been classified into bands mainly by following the transitions with relatively large B(E2).

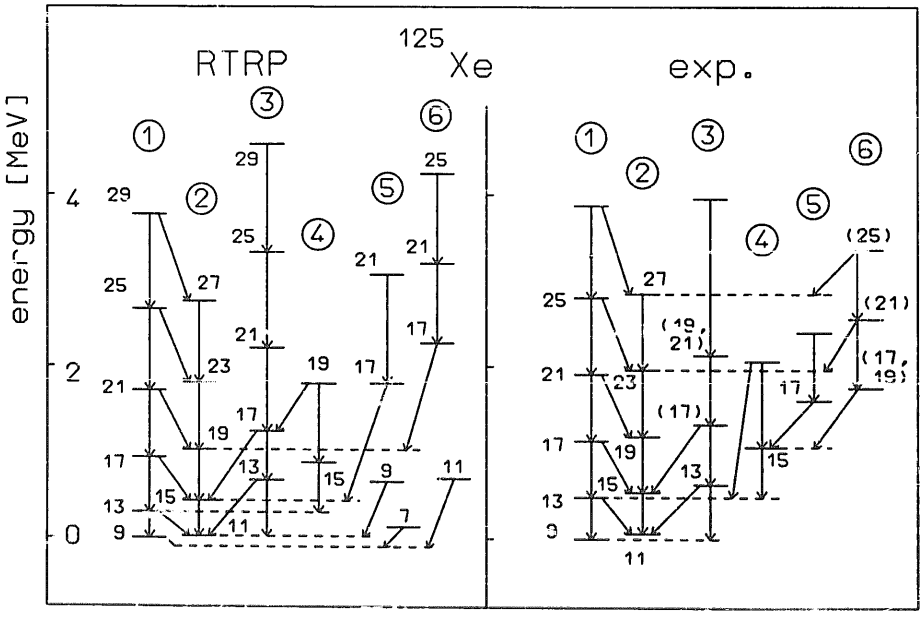

Fig. 1. Experimental and excited negative-parity levels of ^{125}Xe calculated with the VMI-RTRP model (parameters: see table 1).

Fig. 2 displays the Nilsson diagram of single-particle orbitals. Up to 15 single-particle orbitals have been considered. However, only the $1h_{11/2}$, $2f_{7/2}$, and $1h_{9/2}$ spherical orbitals appear in the wave functions with sizable amplitudes. Table 2 shows the strong dominance of $1h_{11/2}$ orbitals. The energy fit is fairly good.

One can, however, ask to what extent the goodness of the fit depends on γ and whether a non-trivial deviation from axial symmetry is really necessary. To this purpose, let us examine the γ-dependence of the calculated yrast-excitation energies (fig. 3). A striking feature of the experimental spectra is the near degeneracy of the favoured and unfavoured states; as a matter of fact, this feature appears in all odd-A isotopes from ^{123}Xe to ^{133}Xe. As can be seen in fig. 3, this property is reproduced by the calculated spectrum in a narrow γ-interval around $\gamma = 30°$. The level sequence in the case of axial symmetry is either a strongly coupled type (prolate), or similar to the rotation-aligned type (oblate). This observation constitutes an argument in favour of triaxial deformation. It is true that for $I \geq \frac{17}{2}$ the favoured and unfavoured yrast states are also degenerate at $\gamma = 60°$. However, at this deformation the electromagnetic properties are not satisfactorily described. In particular, the yrast

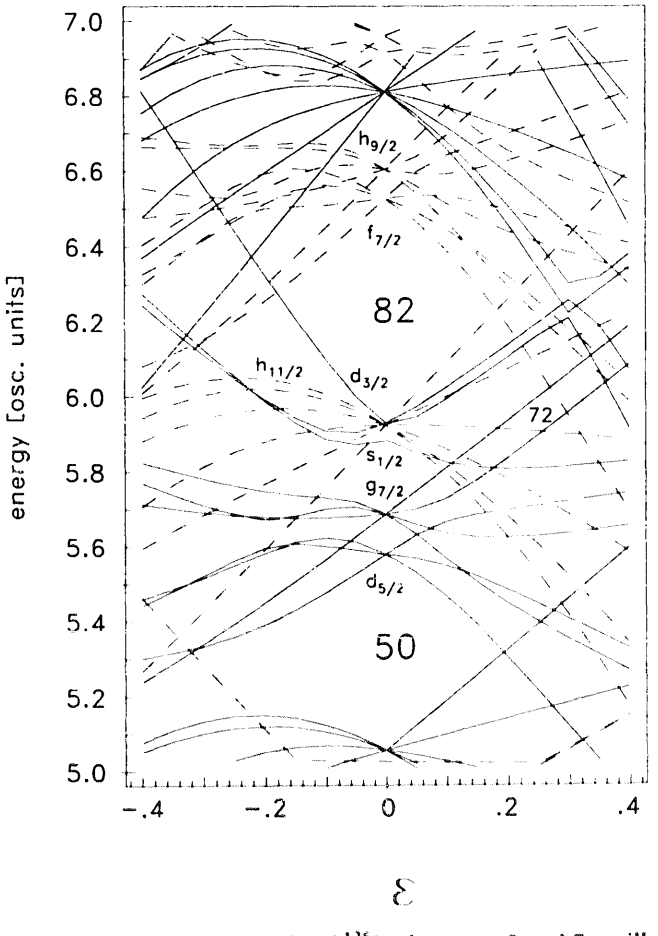

Fig. 2. Nilsson diagram of single-particle orbitals of ^{125}Xe between 5 and 7 oscillator shells (1 oscillator shell is ≈8.5 MeV for ^{125}Xe).

TABLE 2

Relative single-particle structure of negative-parity states in ^{125}Xe calculated with the RTRP model (parameters: $\varepsilon = 0.25$, $\gamma = 24°$ and see table 1). For each spin the squared amplitude is given for the four lowest levels.

	1st level			2nd level			3rd level			4th level		
Spin	$h_{11/2}$	$f_{7/2}$	$h_{9/2}$	$h_{11/2}$	$f_{7/2}$	$h_{9/2}$	$h_{11/2}$	$f_{7/2}$	$h_{9/2}$	$h_{11/2}$	$f_{7/2}$	$h_{9/2}$
$\frac{9}{2}$	91.0	7.4	0.8	90.7	7.6	0.8	83.9	8.8	4.2	16.6	23.6	36.6
$\frac{11}{2}$	90.5	7.8	0.8	89.6	8.3	0.9	89.9	7.9	1.0	89.4	8.2	1.1
$\frac{13}{2}$	90.9	7.4	0.7	90.6	7.6	0.9	90.1	8.1	0.8	8.9	25.1	41.4
$\frac{15}{2}$	89.5	8.4	0.9	90.6	7.6	0.8	89.8	8.2	0.9	89.6	0.8	0.9
$\frac{17}{2}$	90.8	7.4	0.8	90.0	8.1	0.9	89.5	8.5	0.8	11.3	25.3	38.5
$\frac{19}{2}$	88.9	8.8	1.0	90.2	7.9	0.8	89.9	8.1	0.8	88.8	8.8	1.0
$\frac{21}{2}$	90.6	7.5	0.9	88.9	8.8	1.0	87.3	8.9	1.8	12.9	25.6	36.3
$\frac{23}{2}$	88.3	9.1	1.1	89.9	8.1	0.8	90.3	7.8	0.8	87.9	9.4	1.2
$\frac{25}{2}$	90.4	7.7	0.9	88.2	9.3	1.1	12.1	26.1	36.1	87.1	8.7	2.4
$\frac{27}{2}$	87.8	9.4	1.2	89.8	8.2	0.8	90.3	7.8	0.9	85.6	10.1	2.0
$\frac{29}{2}$	90.1	7.8	1.0	87.7	9.5	1.2	10.6	26.6	36.5	88.7	8.3	1.6

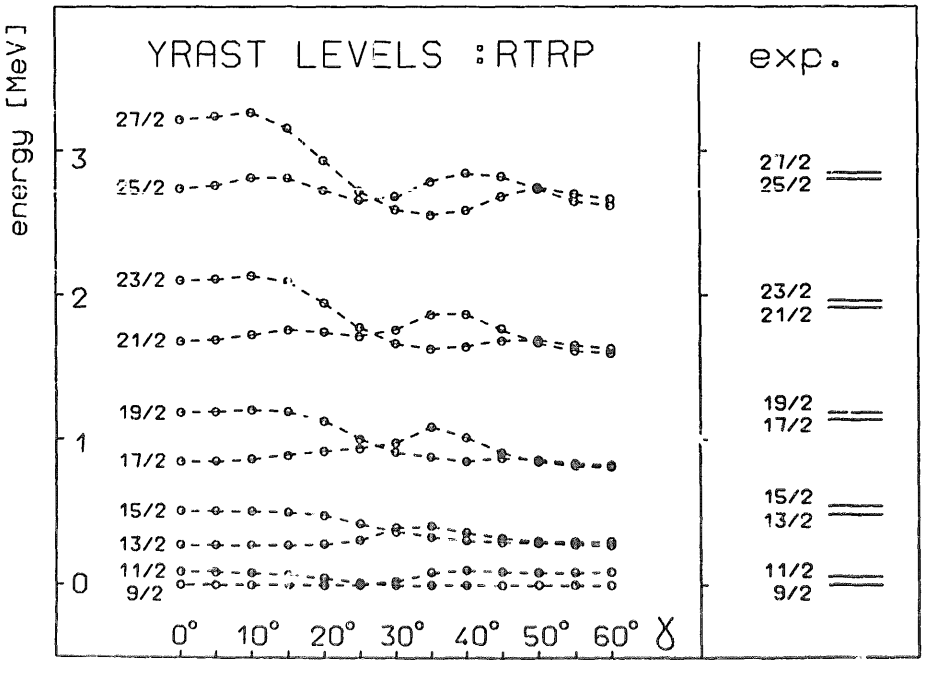

Fig. 3. Gamma-dependence of yrast excitation energies in ^{125}Xe ($\pi = -$) calculated with the VMI-RTRP model (parameters: $\varepsilon = 0.25$ and see table 1).

unfavoured-to-favoured transitions are too weak in the calculations, and the decay pattern of the yrare states cannot be reproduced at $\gamma = 60°$ (see table 4). Furthermore, the position and signature splitting of the yrare band is very sensitive to γ, and cannot be understood with an oblate shape. This sensitivity is a direct reflection of the large contribution from the core γ-band to these states, as is discussed below. Note also that the present calculation ($\gamma = 24°$) can at the same time easily describe the$(j-1)$ anomaly, i.e. the location of the $\frac{9}{2}^-$ state under the $\frac{11}{2}^-$ one.

At this point we want to make a comment on the relative large value of the deformation parameter $\varepsilon = 0.25$, which is larger than the value $\varepsilon = 0.19$ assumed for the even-even core [19]). It was chosen in order to get the energetic ordering of the yrast band, i.e. to reproduce the $\frac{9}{2}^-$ state below the $\frac{11}{2}^-$ state, and also to get the near degeneracy of the favoured and unfavoured states. From the measured lifetime $\tau = 12.5 \pm 1.3$ ps of the $\frac{15}{2}^-_1$ level a value $B(\mathrm{E2}; \frac{15}{2}^-_1 \rightarrow \frac{11}{2}^-_1) = 0.24\,(e \cdot \mathrm{b})^2$ can be deduced [20]). It can be reproduced at $\varepsilon = 0.21$ and $\gamma = 24°$, but then the predicted $\frac{11}{2}^-$ state is below the $\frac{9}{2}^-$ state. If one introduces Coriolis attenuation the right ordering of the levels can be obtained, but then the lifetime of the above-mentioned transition increases drastically. With the used deformation parameters, i.e. $\varepsilon = 0.25$ and $\gamma = 24°$, and no Coriolis attenuation the calculated transition strength is $B(\mathrm{E2}; \frac{15}{2}^-_1 \rightarrow \frac{11}{2}^-_1) = 0.34\ (e \cdot \mathrm{b})^2$ ($\tau = 8.8$ ps). This lifetime is slightly below the observed value. An explanation for the rather large value of ε is that the $h_{11/2}$ shell is a little bit too low with the standard κ and μ and the Fermi level lies too high thus leading to an artificially large deformation parameter ε. In order to have not too many free parameters we take the standard values for κ and μ [ref. [16])]. It is possible that a calculation with a more realistic potential will give deformation parameters closer to those of the even-even core.

Let us now examine the yrare states with both signatures; the states with $I = \frac{11}{2}, \frac{15}{2}, \frac{19}{2}, \ldots$ have the favoured signature * $\alpha = -\frac{1}{2}$; the unfavoured states with $\alpha = \frac{1}{2}$ are those with $I = \frac{9}{2}, \frac{13}{2}, \frac{17}{2}, \ldots$. Most unusually, the yrare favoured states known so far are located above the position they would occupy in the strongly coupled case, i.e. the signature splitting is inverted with respect to what a cranking calculation would have predicted. Moreover, a connection between triaxiality and signature inversion has been discussed in ref. [21]). While the number of observed yrare states is pretty small, one can extend the theoretical calculation to higher spins.

The RTRP calculation indeed predicts an inversion of the signature splitting around $I = \frac{27}{2}$–$\frac{33}{2}$. Above this angular momentum, the signature splitting behaves as predicted by one-dimensional cranking (fig. 4). A transition from a triaxial regime at low spins to a cranking regime at high spins has been predicted by Hamamoto [22]). In the triaxial regime, the core angular momentum is not completely aligned along the axis with the largest moment of inertia (the 2-axis for $\gamma = 30°$). In the cranking regime the core angular momentum is aligned along the cranking axis. As a matter of fact, only yrast states have been considered in ref. [22]).

* We use signature as a label defined by $\alpha = I \bmod 2$.

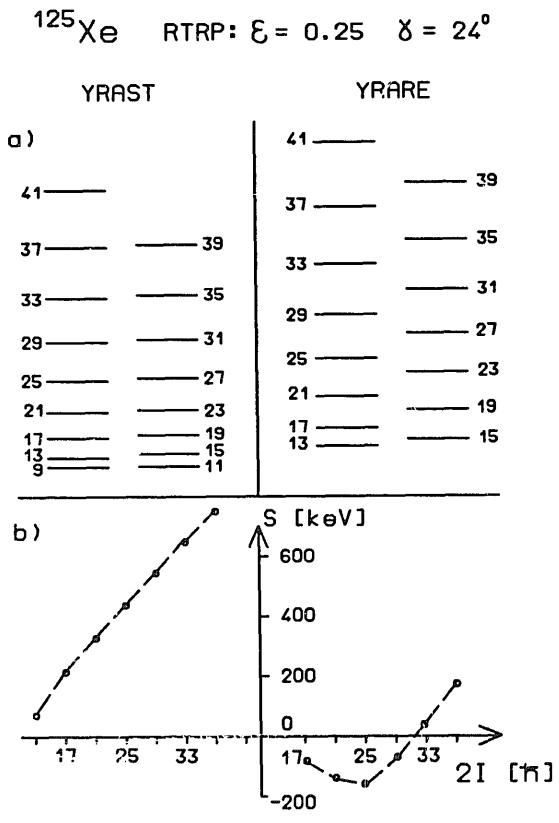

Fig. 4. (a) Negative-parity yrast and yrare energy levels of ^{125}Xe calculated with the RTRP model (parameters: see table 1). (b) Signature splitting S vs. spin. The hypothetical strong coupling positions of the unfavoured states have been calculated by assuming an energy sequence which follows the $I(I+1)$ law. S is the difference between the actual energy and the calculated strong-coupling energy of the unfavoured state.

We can also follow the transition by examining the amplitudes of the core states in the wave functions (fig. 5). These amplitudes are easily obtained from the matrix elements $\langle IMK\nu|IMR\alpha Nlj\rangle$ which were discussed above in connection with the VMI option. Squared amplitudes for both yrast and yrare states with $I = \frac{13}{2}, \frac{15}{2}, \frac{25}{2}, \frac{27}{2}$ are represented. The $2_2^+, 3_1^+, 4_2^+, \ldots$ core states form the quasi-γ-band of a triaxial rotor; there is no β-band of the core in this model. In the vicinity of $\gamma = 30°$ one can safely use the concept of ground state and γ-band, since inter-band electromagnetic transitions are weak compared to intra-band transitions. The amplitudes of components from the γ-band in the yrast states are pretty small. As can be seen in fig. 5b, the probability that the core is in the ground band is larger than 90% in both favoured and unfavoured states. The situation is different in the yrare case. The γ-band components are strong in the unfavoured states at both low and high spin. Starting from $I = \frac{17}{2}$, the main component of the wave function comes from an odd spin member of the γ-band. The angular momentum of this component and j are stretched. At the same time, the difference in structure between low-spin and high-spin favoured states is striking. At low spin there is a large contribution from

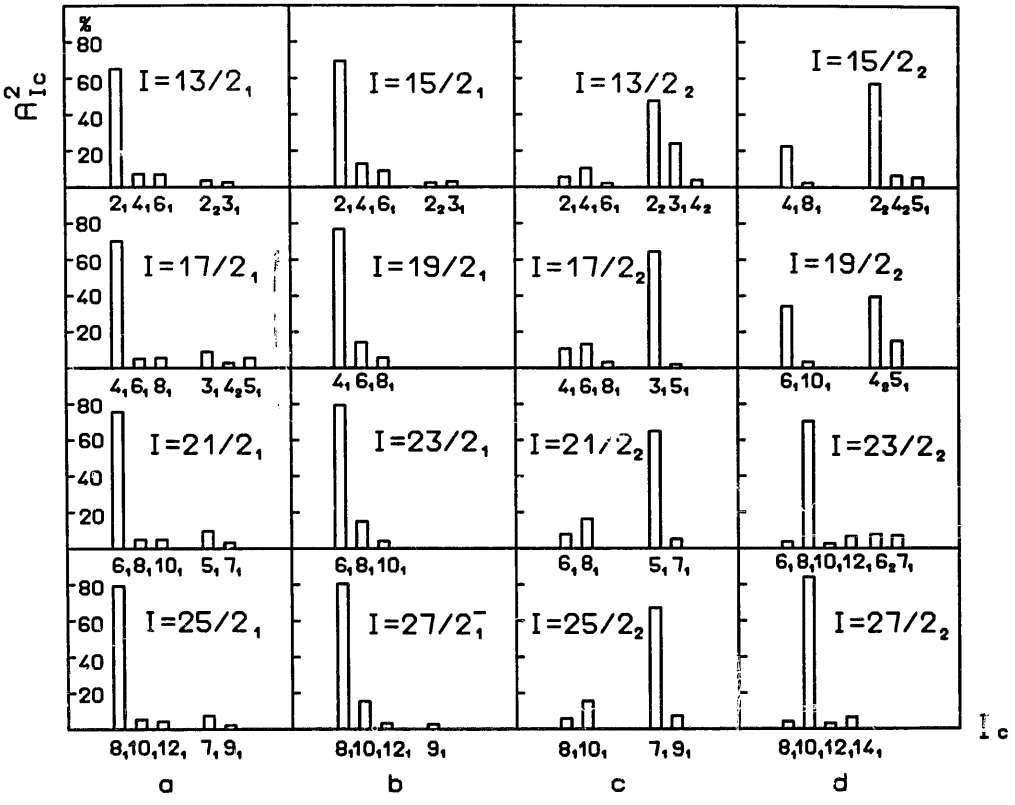

Fig. 5. Squared amplitudes A^2_{Ic} of core states for yrast and yrare ($\pi = -$) of ^{125}Xe calculated with the RTRP model. Same parameters as in fig. 1: (a) yrast favoured, (b) yrast unfavoured, (c) yrare favoured, (d) yrare unfavoured.

γ-band states which practically disappears at high spin. Correspondingly, the ground band contribution increases steadily with angular momentum. One can assume that both changes in the contribution of the γ-band are related to the signature inversion at low spin. An interesting question in the present calculation is then how close the different rotational bands come to full alignment, i.e. if the $\boldsymbol{R}$-vector and the $\boldsymbol{j}$-vector, respectively are close to the 2-axis. It seems evident that in general, this alignment will become stronger with increasing spin. A problem with these components is that they are defined along a body-fixed axis and the physical significance might therefore be somewhat questionable. From this point of view, the projection of e.g. $\boldsymbol{j}$ on $\boldsymbol{R}$ might be a more proper measure of the alignment. On the other hand, such quantities do not give any idea of the rotation axis relative to the intrinsic axis and are less illustrative from this point of view. Below we will consider several of these quantities to try to understand how the rotational vector is built at large triaxiality.

The quantity $\langle \boldsymbol{R} \cdot \boldsymbol{j} \rangle / |\boldsymbol{R}|$ gives direct information on the particle alignment, defined as the projection of the particle angular momentum on the rotation axis. The behaviour of the yrast states (see fig. 6) is similar to what happens in the axially symmetric case, viz. the favoured states have a larger alignment than the unfavoured ones. On the contrary, starting from $I = \frac{17}{2}$, the unfavoured yrare states have a larger

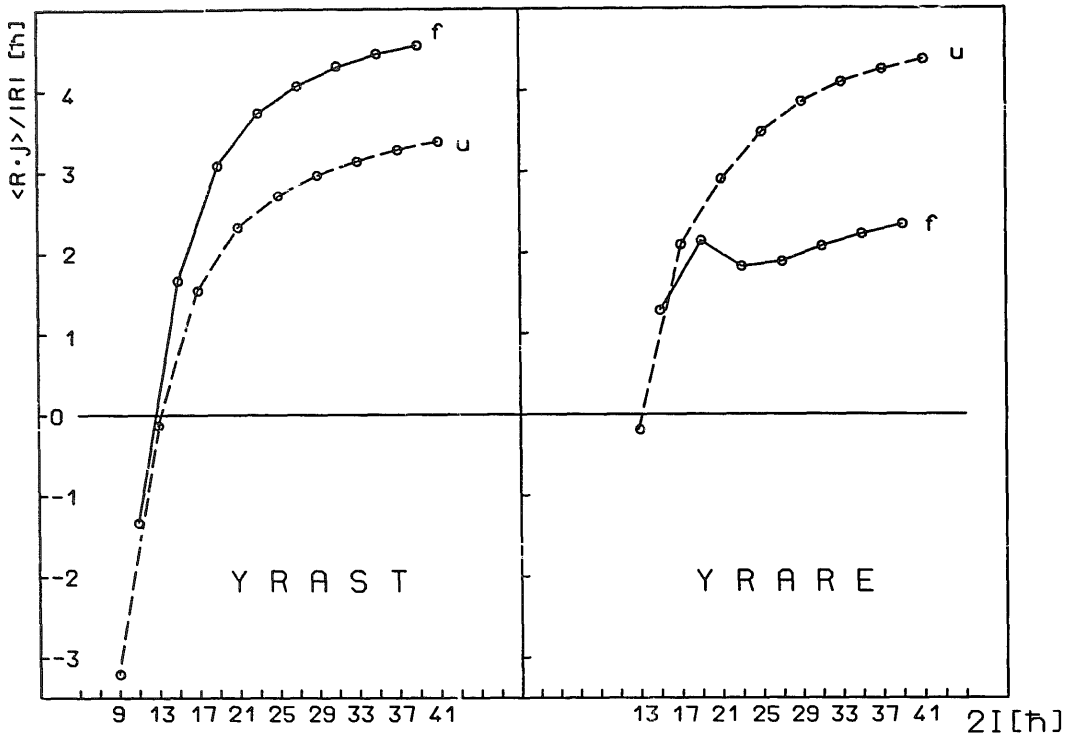

Fig. 6. Particle alignment $\langle \boldsymbol{R} \cdot \boldsymbol{j} \rangle / |\boldsymbol{R}|$ vs. spin of yrast and yrare states ($\pi = -$) of ^{125}Xe calculated with the RTRP model (parameters: see table 1): f: favoured; u: unfavoured.

alignment than the favoured ones. At $I = \frac{17}{2}$ the particle angular momentum is coupled to the $R = 3$ state of the γ-band, which is also the minimum allowed value of $\boldsymbol{R}$. The favoured states with $I > \frac{19}{2}$ have as the strongest core component a state belonging to the ground band with an angular momentum $\boldsymbol{R}$ which is not parallel to $\boldsymbol{j}$.

Since states belonging to the γ-band have a smaller alignment along the 2-axis of the rotational angular momentum $\boldsymbol{R}$ compared to the ground band, let us have a look at the projection R_2 on the axis with the largest moment of inertia. A plot of $\sqrt{\langle R_2^2 \rangle}$ for both yrast and yrare is shown in fig. 7a. Fig. 7b shows $\sqrt{\langle R_1^2 \rangle + \langle R_3^2 \rangle}$, i.e. the projection of $\boldsymbol{R}$ in the plane perpendicular to the 2-axis. At small I-values, the projection of $\boldsymbol{R}$ on the perpendicular plane is relative large, especially for the unfavoured states. One can see that there is a crossing of the yrare favoured and unfavoured curves in the vicinity of $I = \frac{19}{2}$. We are tempted to assume that this phenomenon is also related to the change occurring in the wave functions.

Calculated yrare states for $\gamma = 0°$ and $\gamma = 24°$ with $\varepsilon = 0.25$ are shown in fig. 8. At first sight one could think that a signature inversion is present also in the case of axial symmetry. In fact, a closer look at the wave function shows that the yrare states at $\gamma = 0°$ are dominated by the $h_{9/2}$ component, i.e. in reality it is the band with signature $\alpha = \frac{1}{2}$ ($I = \frac{9}{2}, \frac{13}{2}, \ldots$) which becomes favoured (table 3). Besides, a calculation with $\gamma = 0°$ fails to reproduce correctly the excitation energies. It is interesting to notice that at $\gamma = 0°$ the states with signature $\alpha = \frac{1}{2}$ also remain favoured

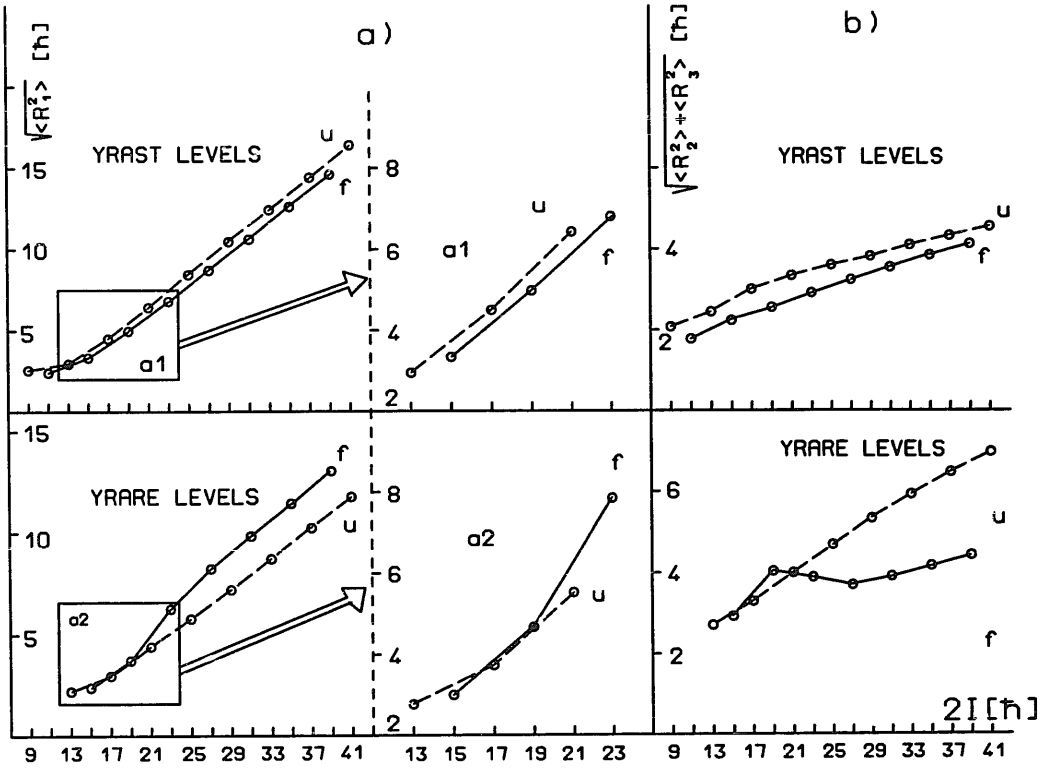

Fig. 7. (a) Square root of the average value of the squared projection R_2^2 on the 2-axis of yrast and yrare levels ($\pi = -$) of ^{125}Xe calculated with the RTRP model (parameters: see table 1). (b) Square root of average value of the squared projection of R^2 on a plane perpendicular to the 2-axis.

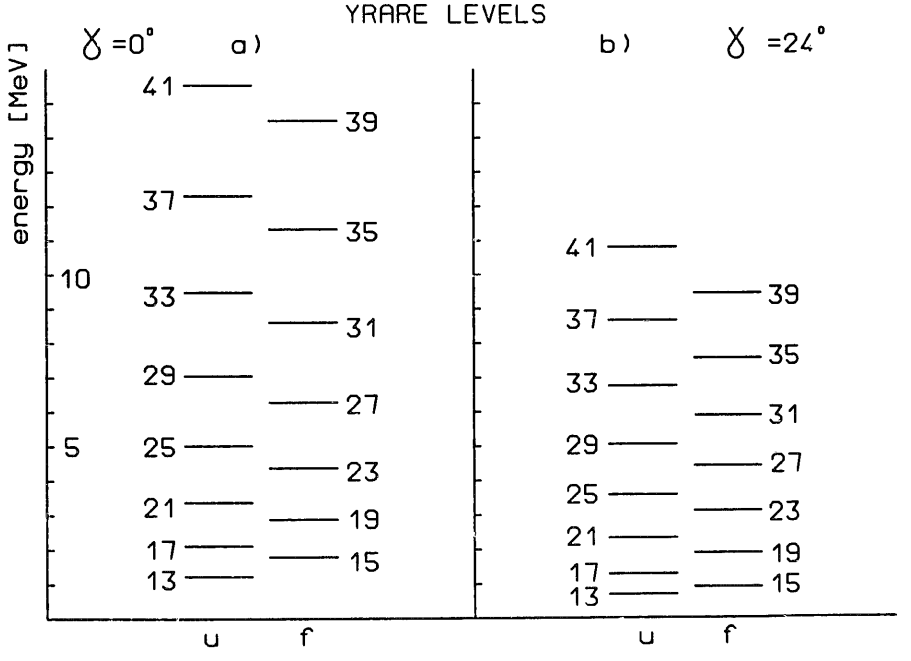

Fig. 8. Calculated yrare levels for $\gamma = 0°$ and $\gamma = 24°$ of yrast and yrare states ($\pi = -$) of ^{125}Xe calculated with the RTRP model (other parameters: see table 1).

TABLE 3

Relative single-particle structure (squared amplitude) for yrare band ($\pi = -$) of ^{125}Xe for axial shape calculated with the RTRP model (parameters: $\varepsilon = 0.25$, $\gamma = 0°$ and see table 1)

I	$h_{11/2}$	$h_{9/2}$	$f_{7/2}$
$\frac{9}{2}$	0.09	0.35	0.22
$\frac{11}{2}$	0.44	0.19	0.16
$\frac{13}{2}$	0.09	0.38	0.23
$\frac{15}{2}$	0.77	0.06	0.10
$\frac{17}{2}$	0.08	0.39	0.23
$\frac{19}{2}$	0.83	0.04	0.08
$\frac{21}{2}$	0.08	0.40	0.24

at high spin. On the contrary, in the triaxial case the signature splitting changes sign around $I = \frac{31}{2}$, which corresponds to the transition from triaxial to the cranking regime seen also in the behaviour of the rotation matrix elements (see fig. 7b).

Moreover, the gradual alignment of the total angular momentum in the $\gamma = 30°$ case can be seen in fig. 9, where the squared amplitudes A_K^2 and A_Ω^2 are plotted

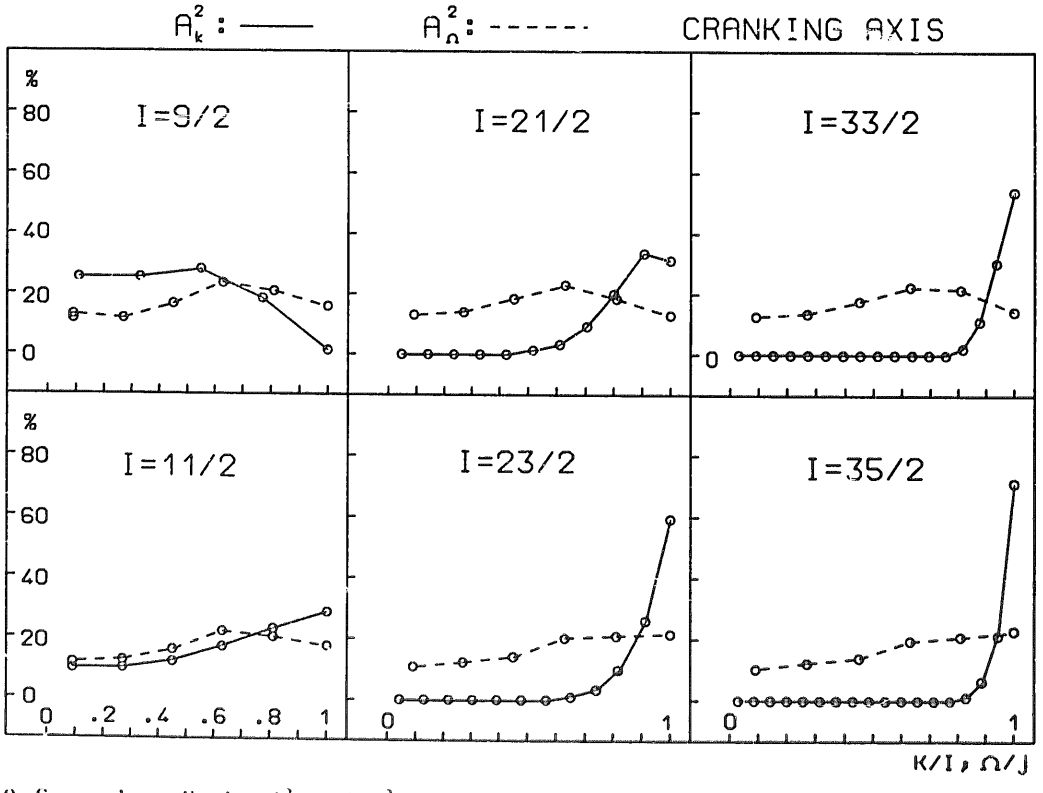

Fig. 9. Squared amplitudes A_K^2 and A_Ω^2 of projection quantum number K and Ω vs. the degrees of alignment K/I and Ω/j, respectively for the yrast states ($\pi = -$) of ^{125}Xe calculated with the RTRP model (parameters: see table 1). The quantization axis has been rotated so as to coincide with the axis with the largest moment of inertia.

versus the quantity K/I and Ω/j, respectively. The quantization axis-3 has been made to coincide with the axis with the largest moment of inertia. One can see the gradual transition from a wide distribution of K/I at low spin to a narrow one at $I=\frac{31}{2}$. (Note that the single-particle alignment Ω/j has a rather wide distribution which remains almost constant with the increase of total spin. This observation is valid also for the yrare wave function.)

This complex behaviour is probably the result of two opposite trends which appear in the triaxial case [1]). On the one hand the core will try to rotate around the axis with the largest moment of inertia (2-axis) and the Coriolis force will favour states with aligned particle angular momentum. This trend is dominant at high spin (cranking regime). At low spin the situation will be dominated by the particle-core overlap energy (mean field energy) which will try to align the particle angular momentum parallel to an axis perpendicular to the 2-axis. At $\gamma=30°$ the shortest axis of the spheroid is the 1-axis. If we look from this direction the nucleus looks nearly oblate and the particle will have the largest overlap with the core if its angular momentum is aligned along the 1-axis. This mechanism has been discussed in ref. [1]). In this case, the rotational angular momentum will also have a component along an axis with smaller moment of inertia. This possibility of rotating around two different principal axes also explains the richness of the triaxial rotor spectrum compared to the axially symmetric one.

Another typical feature of the experimental spectra is the relatively large number of excited bands. We can see four $I=\frac{17}{2}$ states in the level scheme of ^{125}Xe. The RTRP calculation generates several bands containing $\frac{17}{2}$ states. The energies of these states are reproduced quite well, whereas we were not able to reproduce the decay properties. If the calculation is carried out assuming either $\gamma=0°$ or $\gamma=60°$, then these excited bands lie much higher than observed experimentally.

3.2. ELECTROMAGNETIC TRANSITIONS

It has been shown by Hamamoto and Mottelson [23]) that the signature dependence of $B(E2; I \to I-1)$ provides a typical signature of triaxiality.

In order to understand qualitatively this phenomenon, let us consider the schematic case $\gamma=30°$. The static quadrupole moment (diagonal E2 matrix element) vanishes for this value of γ [ref. [1])]. We will first consider a favoured-to-unfavoured yrast transition, e.g. $\frac{15}{2}^+ \to \frac{13}{2}^+$. The wave functions of fig. 5 show that the main core component in both wave functions is 2_1^+. As a result the E2 transition will occur only between other, weaker components (as e.g. $4_1^+ \to 2_1^+$). On the contrary, the unfavoured-to-favoured $\frac{13}{2}^+ \to \frac{11}{2}^+$ transition will be dominated by $2_1^+ \to 0_1^+$, i.e. by an allowed transition between two strong core components. This staggering is typical for triaxiality and has indeed been observed experimentally [24]). A similar effect is also predicted by the interacting boson-fermion model [25]). In the axially symmetric case the core states are strongly mixed. This can be easily seen if the core state

amplitudes in a strongly coupled state with good K are calculated by using formula (4A-6) of ref.[14]). As a consequence the staggering disappears. The calculated staggering behaviour of $B(\mathrm{E2}; I \to I-1)$ is shown in fig. 10.

The behaviour of M1 transitions is exactly opposite. Since the M1 operator cannot change the core angular momentum R, the only transitions that will be strong are those for which the initial and final states have the same dominant components. For example, $B(\mathrm{M1}; \frac{19}{2} \to \frac{17}{2})$ should be large since both states have essentially the same distribution of core components. On the contrary, the $\frac{17}{2} \to \frac{15}{2}$ M1 transition is hindered because the core distributions of the initial and final states are different. This staggering in the $B(\mathrm{M1})$'s is also a reflection of the staggering of the projection $\langle \boldsymbol{R} \cdot \boldsymbol{j} \rangle / |\boldsymbol{R}|$, as implied in Dönau's semiclassical formalism[26]). The staggering of $B(\mathrm{M1})$ which is also present in the axially symmetric case, bears no relation to triaxiality, in contrast to $B(\mathrm{E2}; I \to I-1)$.

Since the staggering in $\langle \boldsymbol{R} \cdot \boldsymbol{j} \rangle / |\boldsymbol{R}|$ found in the yrare states and the energy signature splitting look quite different from yrast, it is interesting to examine the behaviour of E2 and M1 transitions. The main feature of the wave functions of states with "unfavoured" signature starting from $\frac{17}{2_2}$ is the dominance of a core component with odd R, belonging to the quasi-γ band. Thus the core and particle angular momenta are stretched, e.g. $R=7$ and $j=\frac{11}{2}$ in the state $\frac{25}{2_2}$ and the alignment $\langle \boldsymbol{R} \cdot \boldsymbol{j} \rangle / |\boldsymbol{R}| = 3.48$. If we call the stretched states "favoured" then we find that the spin sequence for "favoured" and "unfavoured" states is opposite to the one in yrast.

The behaviour of $B(\mathrm{E2}; I \to I-1)$ shown in fig. 11 can be easily explained by examining the transition between the dominant core components in the wave function, in a manner similar to yrast.

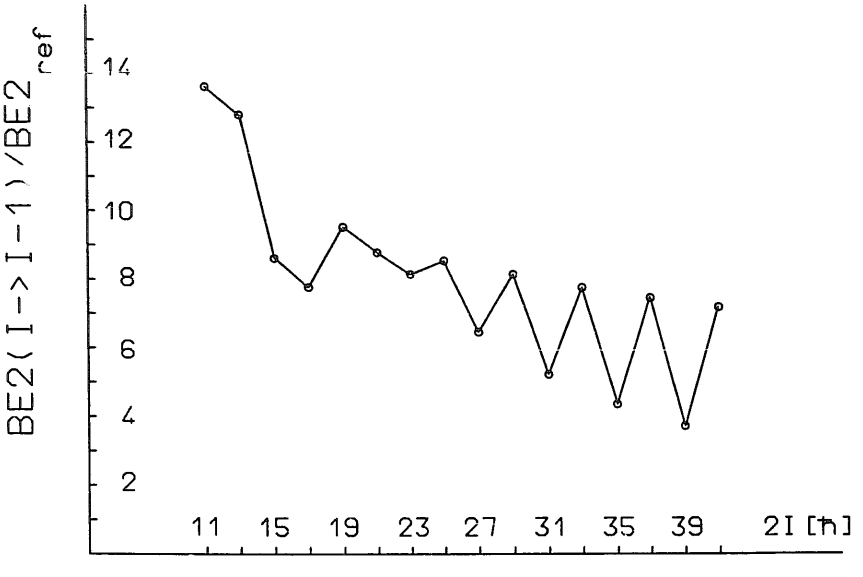

Fig. 10. Signature effect in $B(\mathrm{E2}; I \to I-1)$ between yrast states ($\pi = -$) of ^{125}Xe (parameters: $\varepsilon = 0.25$, $\gamma = 24°$ and see table 1) calculated with the RTRP model. The $B(\mathrm{E2})$ values are expressed in $\mathrm{BE2_{ref}}$ units which are the $B(\mathrm{E2}; I \to I-\Delta I)$ values unperturbed by rotation: $\mathrm{BE2_{ref}} = (5/16\pi)e^2 Q_0^2 \langle IK20 | I-\Delta I, K\rangle^2$ with $K=\frac{7}{2}$ and $Q_0 = 100\,\mathrm{fm}^2$.

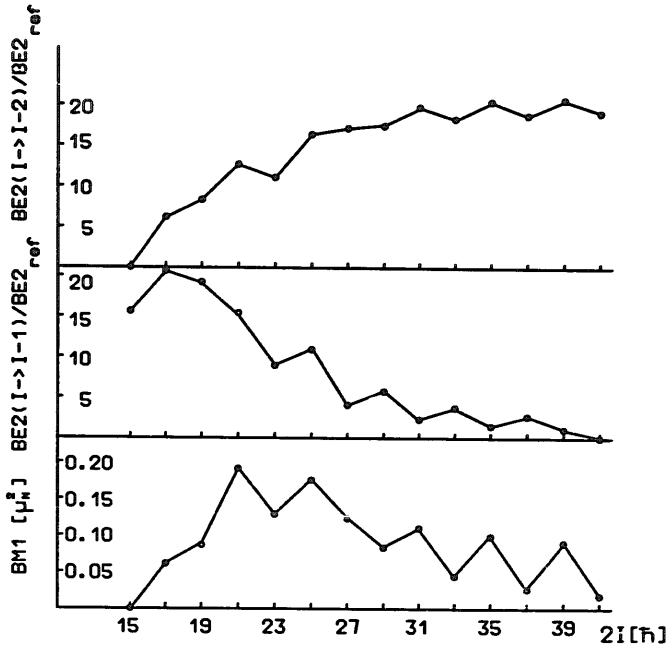

Fig. 11. Signature effect in $B(E2; I \to I-2)$, $B(E2; I \to I-1)$ and $B(M1)$ between yrare states ($\pi = -$) of ^{125}Xe calculated with the RTRP model (parameters: see table 1). See also caption to fig. 10.

The pattern of the calculated $B(M1)$'s (fig. 11) is not nearly as pronounced as for the yrast band. The small staggering that is present at the bottom of the yrare band is inverted compared to yrast and, furthermore, the staggering resumes the normal phase (same as yrast) around $I = \frac{29}{2}$, i.e. in the region where the signature splitting resumes its normal sign (fig. 4). The $B(M1)$ staggering certainly does not follow the calculated alignment $\langle \boldsymbol{R} \cdot \boldsymbol{j} \rangle / |\boldsymbol{R}|$ as expected on the basis of ref. [26]). The latter picture is useful only if it is known that the core angular momentum is essentially the same in the two sets of states (favoured and unfavoured).

Also interesting are the strong out-of-band $B(M1)$'s that are predicted for yrare states. These fall into two categories: (i) transitions from yrare state I to yrast state $I+1$ and (ii) transitions from yrare state I to the third state of spin $I-1$. These $B(M1)$'s are stronger than those within the yrare band in almost every case.

The reason can again be found in the core state distribution; e.g. the yrare states $\frac{23}{2}$, $\frac{27}{2}$ have core distributions similar to those of the yrast states $\frac{25}{2}$, $\frac{29}{2}$, etc. Thus strong M1 transitions should be expected between these states. M1 transitions belonging to (ii) are weaker than those belonging to (i) and represent transitions to states which most closely resemble the core distributions of the yrare states $\frac{17}{2_2}$, $\frac{21}{2_2}$, etc. The final states are $\frac{15}{2_3}$, $\frac{19}{2_3}$ and these are probably the states which should properly be regarded as signature partners of the yrare sequence $\frac{17}{2}$, $\frac{19}{2}$, ... Finally, we note that the very large out-of-band $B(M1)$'s calculated for the yrare sequence $\frac{19}{2}$, $\frac{23}{2}$, ... provide a natural explanation for the non-observance of these states experimentally.

The experimental observation of the B(E2) and B(M1) staggering effect requires at least a good knowledge of E2/M1 mixing ratios. This information is so far very scarce in odd-A Xe. A better knowledge of δ(E2/M1) represents a challenge for future experiments. This phenomenon can anyway not be observed in ^{125}Xe because the yrast favoured-to-unfavoured transitions are much too weak owing to the near

TABLE 4

Branching ratios of negative-parity states of ^{125}Xe calculated with the VMI-RTRP model. The theoretical branching ratios were calculated with experimental transition energies.

			Branching ratios		
				VMI-RTRP	
Level	Spin	Transition	Exp.	$\gamma = 24°$	$\gamma = 60°$
736.7	$\frac{13}{2}^-_1$	426.4 → $\frac{11}{2}^-_1$	100	100	100
		484.2 → $\frac{9}{2}^-_1$	37 ± 14	46	271
893.3	$\frac{13}{2}^-_2$	583.0 → $\frac{11}{2}^-_1$	100	100	100
		640.9 → $\frac{9}{2}^-_1$	94 ± 35	179	8
1310.0	$\frac{15}{2}^-_2$	416.8 → $\frac{13}{2}^-_2$	28 ± 10	62	196
		513.4 → $\frac{15}{2}^-_1$	13 ± 6	14	2
		573.4 → $\frac{13}{2}^-_1$	100	100	100
		999.8 → $\frac{11}{2}^-_1$	not obs.	15	2
1387.6	$\frac{17}{2}^-_1$	591.2 → $\frac{15}{2}^-_1$	100	100	100
		651.0 → $\frac{13}{2}^-_1$	87 ± 30	129	405
1580.0	$\frac{17}{2}^-_2$	269.9 → $\frac{15}{2}^-_2$	5 ± 2	9	5
		686.4 → $\frac{13}{2}^-_2$	100	100	100
		784.1 → $\frac{15}{2}^-_1$	35 ± 15	70	32
		843.3 → $\frac{13}{2}^-_1$	not obs.	15	2
2166.4	$\frac{21}{2}^-_1$	725.4 → $\frac{19}{2}^-_1$	82 ± 34	43	14
		778.7 → $\frac{17}{2}^-_1$	100	100	100
2384.8	$(\frac{21}{2}^-_2)$ [a]	378.5 → $(\frac{17}{2}^-_4)$ [a]	19 ± 9	≤0.1	≤0.1
		804.9 → $\frac{17}{2}^-_2$	100	100	100
		943.6 → $\frac{19}{2}^-_1$	13 ± 6	4	11
3054.7	$\frac{25}{2}^-_1$	839.3 → $\frac{23}{2}^-_1$	82 ± 42	29	9
		888.5 → $\frac{21}{2}^-_1$	100	100	100
4052.4	$(\frac{29}{2}^-_1)$ [a]	953.1 → $\frac{27}{2}^-_1$	99 ± 51	21	7
		997.4 → $\frac{25}{2}^-_1$	100	100	100

[a] Experimentally this level has either no spin assignment or no unique spin assignment. All energies are given in keV.

degeneracy of the levels. Nevertheless, we notice (see table 4) that the unfavoured-to-favoured transitions are indeed rather strong compared to intra-band $\Delta I = 2$ transitions.

There is also some information on the branching ratios. A comparison of experimental and calculated values is given in table 4. With a few exceptions, the agreement is satisfactory.

4. Summary

In conclusion, energy levels and branching ratios in ^{125}Xe have been correctly reproduced by the triaxial rotor plus particle model with $\varepsilon = 0.25$ and $\gamma = 24°$.

The following properties are intimately linked to a substantial deviation from axial symmetry:

(1) The favoured and unfavoured yrast bands are nearly degenerate.

(2) The signature splitting of the yrare bands below $I = \frac{31}{2}$ has the opposite sign to the cranking (or axially symmetric) predictions. Analysis of the wave functions shows that this property is related to the dominance of a core state with odd angular momentum belonging to the quasi-γ band.

(3) The staggering of $B(\mathrm{E2};\ I \to I-1)$ in both yrast and yrare bands appears as a direct consequence of triaxiality and can be explained by the core state distribution in the wave functions. The same is true for $B(\mathrm{M1};\ I \to I-1)$ in the yrare band. Further experimental investigation of $B(\mathrm{E2})$ and $B(\mathrm{M1})$ staggering in transitional nuclei is highly desirable.

The authors would like to thank A. Arima, R. Bengtsson, F. Dönau, S. Frauendorf, I. Hamamoto, W. Lieberz, W. Nazarewicz, J. Rikovska and R. Wyss for stimulating discussions. This work was supported by the German Federal Minister for Research and Technology (BMFT) under contract number 06OK143.

Appendix A

Description of the used parameters:

(1) ε and γ are the deformation parameters of the single-particle potential which is used in the one-body hamiltonian [eq. (2) and ref. [5])]. We used standard Nilsson parameters for the modified oscillator potential [taken from ref. [16])].

(2) The pairing parameters are needed in order to obtain the pairing strength G for the BCS calculation. The expression

$$G \cdot A = G0 + G1 \cdot \frac{N-Z}{A}$$

gives an isospin-dependent pairing strength as introduced in ref. [17]). In table 1 the standard values of $G0$ and $G1$ taken from Nilsson *et al.* [17]) are listed; it should be understood that $\sqrt{15Z}$ and $\sqrt{15N}$ orbitals below and above the Fermi surface are included in the pairing calculation.

(3) The inertial parameter E2PLUS (in MeV) is used in RTRP (not in VMI-RTRP). The parameter B is calculated as

$$\frac{\hbar^2}{B} = 6 \cdot \text{E2PLUS} \frac{\sin^2(3\gamma)}{\frac{9}{2}(3-\sqrt{9-8\sin^2(3\gamma)})} .$$

Then the moment of inertia is ($K = 1, 2, 3$)

$$\frac{1}{\Theta_K} = \frac{\hbar^2}{2B} \frac{1}{4\sin^2(\gamma + \frac{2}{3}K\pi)} .$$

The used value of E2PLUS is around the energy of the first 2^+ states of the neighbouring even-even nuclei.

(4) The VMI parameters are $A00 = (1/2\Theta_{00})$ (in MeV) and STIFF = C (in MeV^3). Θ_{00} and C are the VMI parameters of Mariscotti *et al.*[27]). The VMI-RTRP is an extension of the RTRP. It assumes spin-dependent moments of inertia ($K = 1, 2, 3$):

$$\Theta_{KR} = \tfrac{4}{3}\Theta_{0R} \sin^2(\gamma - \tfrac{2}{3}K\pi) .$$

The facor Θ_{0R} is the moment of inertia of an axially symmetric even-even nucleus with angular momentum R. It can be obtained from the VMI equation in the axially symmetric case

$$\varepsilon_R^3 - \varepsilon_0 \varepsilon_R^2 - \frac{1}{2C} R(R+1) = 0 ,$$

where $\varepsilon_R = \Theta_{0R}/\hbar^2$ and $\varepsilon_0 = \Theta_{00}/\hbar^2$. The above equation results from the minimization of the rotational energy E_R as a function of the moment of inertia Θ_{0R}

$$E_R(\Theta_{0R}) = \frac{\hbar^2}{2\Theta_{0R}} R(R+1) + \tfrac{1}{2}C\left[\frac{\Theta_{0R}}{\hbar^2} - \frac{\Theta_{00}}{\hbar^2}\right]^2$$

and

$$\partial E_R / \partial \Theta_{0R} = 0 .$$

The parameters Θ_{00} and C fix the variation of Θ_{0R} and can be determined for example from the core energies of the first 2^+ and 4^+ states.

References

1) J. Meyer-ter-Vehn, Nucl. Phys. **A249** (1975) 111
2) H. Toki and A. Faessler, Nucl. Phys. **A253** (1975) 231
3) S.E. Larsson, G. Leander and I. Ragnarsson, Nucl. Phys. **A307** (1978) 189
4) I. Ragnarsson and P.B. Semmes, Hyp. Int. **43** (1988) 425 and to be published
5) S.E. Larsson, Phys. Scripta **8** (1973) 17
6) M. Cunningham, Nucl. Phys. **A385** (1982) 204, 221
7) S.T. Hsieh, H.C. Chiang and M.M. King Yen, Phys. Rev. **C41** (1990) 2898
8) S.G. Rohoziński, J. Srebrny and K. Horbaczewska, Z. Phys. **268** (1974) 401
9) R.F. Casten and P. von Brentano, Phys. Lett. **B152** (1985) 22

10) T. Otsuka and M. Sugita, Phys. Rev. Lett. **59** (1987) 1541
11) M. Sugita, T. Otsuka and A. Gelberg, Nucl. Phys. **A493** (1989) 350
12) G. Leander, Nucl. Phys. A273 (1976) 286
13) F. Dönau, J. Hattula, H. Helppi, A. Luukko and M. Jääskeläinen, J. of Phys. **G7** (1981) 1379
14) A. Bohr and B. Mottelson, Nuclear structure, Vol. II (Benjamin, Reading, MA, 1975)
15) A.G. Griffiths *et al.*, to be published
16) Jing-ye Zhang, N. Xu, D.B. Fossan, Y. Liang, R. Ma and E.S. Paul, Phys. Rev. **C39** (1989) 714
17) S.G. Nilsson, C.F. Tsang, A. Sobiczewski, Z. Szymański, S. Wycech, C. Gustafson, I.-L. Lamm, P. Möller and B. Nilsson, Nucl. Phys. **A131** (1969) 1
18) A. Granderath, D. Lieberz, A. Gelberg, S. Freund, W. Lieberz, R. Wirowski, P. von Brentano and R. Wyss, Nucl. Phys. A (1991) accepted for publication
19) S. Raman, C.H. Malarkey, W.T. Milner, C.W. Nestor Jr. and P.H. Stelson, Atomic Data Nucl. Data Tables **36** (1987) 1
20) D. Alber, H. Graw, H. Haas, H.-E. Mahnke, W. Semmler and W.-D. Zeitz, Nucl. Phys. **A413** (1984) 353
21) R. Bengtsson, F.R. May and J.A. Pinston, Proc. XXth Intern. Winter Meeting on Nuclear Physics, Bormio, Italy (1982)
22) I. Hamamoto, Phys. Lett. **B193** (1987) 399
23) I. Hamamoto and B. Mottelson, Phys. Lett. **B132** (1983) 7
24) S. Skoda, J. Busch, J. Eberth, M. Liebchen, T. Myläus, N. Schmal, R. Sefzig and W. Teichert, Proc. Int. Workshop on Nuclear structure of the zirconium region, p. 315, ed. J. Eberth, R.A. Mayer and K. Sistemich, Bad Honnef, 1988 (Springer)
25) N. Yoshida, H. Sagawa, T. Otsuka and A. Arima, Phys. Lett. **B215** (1988) 51; Nucl. Phys. **A503** (1989) 90
26) F. Dönau, Nucl. Phys. **A471** (1987) 469
27) M.A.J. Mariscotti, G. Scharff-Goldhaber and B. Buck, Phys. Rev. **178** (1969) 1864